Electronic supplementary information for

High-throughput design of bimetallic core–shell catalysts for the electrochemical nitrogen reduction reaction

Sooyeon Kim,[1§] Min-Cheol Kim, [2§] Byung Chul Yeo,[3] Sang Soo Han[1]*

[1]Computational Science Research Center, Korea Institute of Science and Technology, Seoul 02792, Republic of Korea
[2]School of Chemical Engineering, Sungkyunkwan University, 2066, Seobu-ro, Jangan-gu, Suwon 16419, Republic of Korea
[3]Department of Energy Resources Engineering, Pukyong National University, Busan 48509, Republic of Korea

*Correspondence to: sangsoo@kist.re.kr (S.S.H)

[§]These authors equally contributed.

Table S1. Lattice parameters of the core metals used in this study. Units in Å.

Element	Crystal structure	Calculated (This study)	Experimental	Exp. reference
Pt	FCC	4.00	3.92	[1]
Pd	FCC	3.99	3.89	[1]
Co	HCP	a = 2.51, c = 4.07	a = 2.51, c = 4.09	[2]
Ni	FCC	3.54	3.51	[3]
Ta	BCC	3.34	3.30	[3]
Ir	FCC	3.89	3.83	[3]
Ru	HCP	a = 2.73, c = 4.32	a = 2.70, c = 4.28	[1]
Al	FCC	4.06	4.02	[3]
Re	HCP	a = 2.76, c = 4.47	a = 2.76, c = 4.46	[4]
Ag	FCC	4.23	4.09	[1]
Au	FCC	4.17	4.08	[1]

[1] *Acc. Chem. Res.* **2016**, 49, 12, 2841–2850.
[2] Proc. Phys. Soc. **1954**, 67, 456-466.
[3] Phy. Rev. B **2009**, 79, 085104.
[4] J. Metals **1955,** 7, 168-179.

Table S2. List of the potential 18 candidates after the second screening process using the descriptor for activity ((ΔG_{*N2H} - ΔG_{*N2}) or (ΔG_{*NH2}- ΔG_{*NH})) and selectivity (ΔG_S). Formation energies of the core-shell catalysts (E_{cs}) are also considered to verify the stability of the selected candidates. E_{cs} is calculated as, $E_{cs} = E_{tot} - E_{core} - N\,\mu_{shell}$, where E_{tot} is the total energy of the core-shell slab system, E_{core} is the total energy of the core slab system, N is number of shell atoms in the given core-shell slab system, and μ_{shell} is the cohesive energy of the shell metal defined as $\mu = (E_{bulk} - N' E_{atom}) / N'$, where E_{bulk} is the total energy of the bulk structure, N' is the number of atoms in the bulk crystal structure, and E_{atom} is the total energy of an isolated atom. For these calculations, a slab model with three core layers and one shell layer was considered.

Core	**Shell**	**(ΔG_{*N2H} - ΔG_{*N2}) or (ΔG_{*NH2}- ΔG_{*NH}) (eV)**	**ΔG_S (eV)**	**E_{CS}/N (eV/atom)**
Pd	Tc	0.47	-0.70	-0.79
Pt	Tc	0.49	-0.62	-0.89
Co	Mn	0.51	-1.21	-1.47
Pd	Re	0.53	-0.65	-1.01
Ni	Mn	0.53	-1.11	-1.49
Ta	Re	0.54	-0.54	-1.21
Pt	Re	0.65	-0.62	-1.13
Pt	Mo	0.74	-0.49	-1.05
Ag	Nb	0.75	-0.61	-0.42
Pd	Mo	0.75	-0.49	-0.96
Ir	Re	0.78	-0.50	-1.23
Pd	W	0.80	-0.56	-0.97
Pd	Os	0.81	-0.71	-0.60
Pd	Ru	0.83	-0.73	-0.49
Rh	Re	0.84	-0.51	-1.17
V	Tc	0.85	-0.49	-1.14
Co	Cr	0.87	-2.09	-1.34
Cu	Fe	0.88	-0.48	-0.98

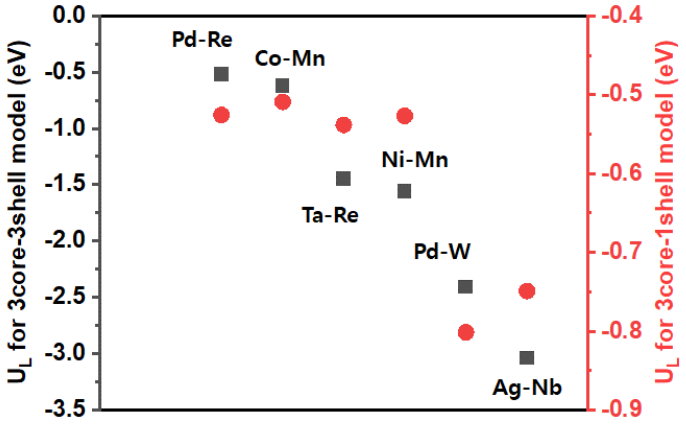

Fig. S1 Comparison of the limiting potential (U_L) calculated using the 3_{core}-3_{shell} model (black squares, from full NRR pathway) and using the 3_{core}-1_{shell} model (red circles, from ((ΔG_{*N2H} - ΔG_{*N2}) and (ΔG_{*NH2}-ΔG_{*NH}))).

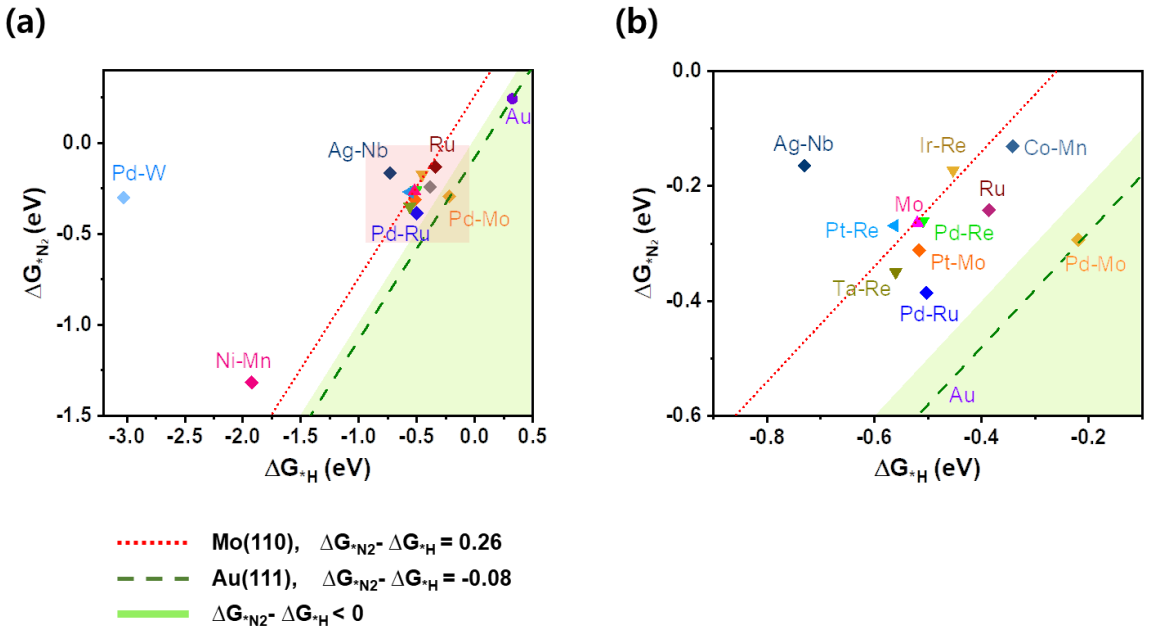

Fig. S2 (a) Free energy changes of $*N_2$ vs. *H for the eleven selected core–shell catalysts. Ru(0001), Au(111) and Mo(110) are additionally considered for comparison. The green-shaded area is where ΔG_{*H} is larger than ΔG_{*N2}. The red-shaded area is enlarged in (b) for clarity.

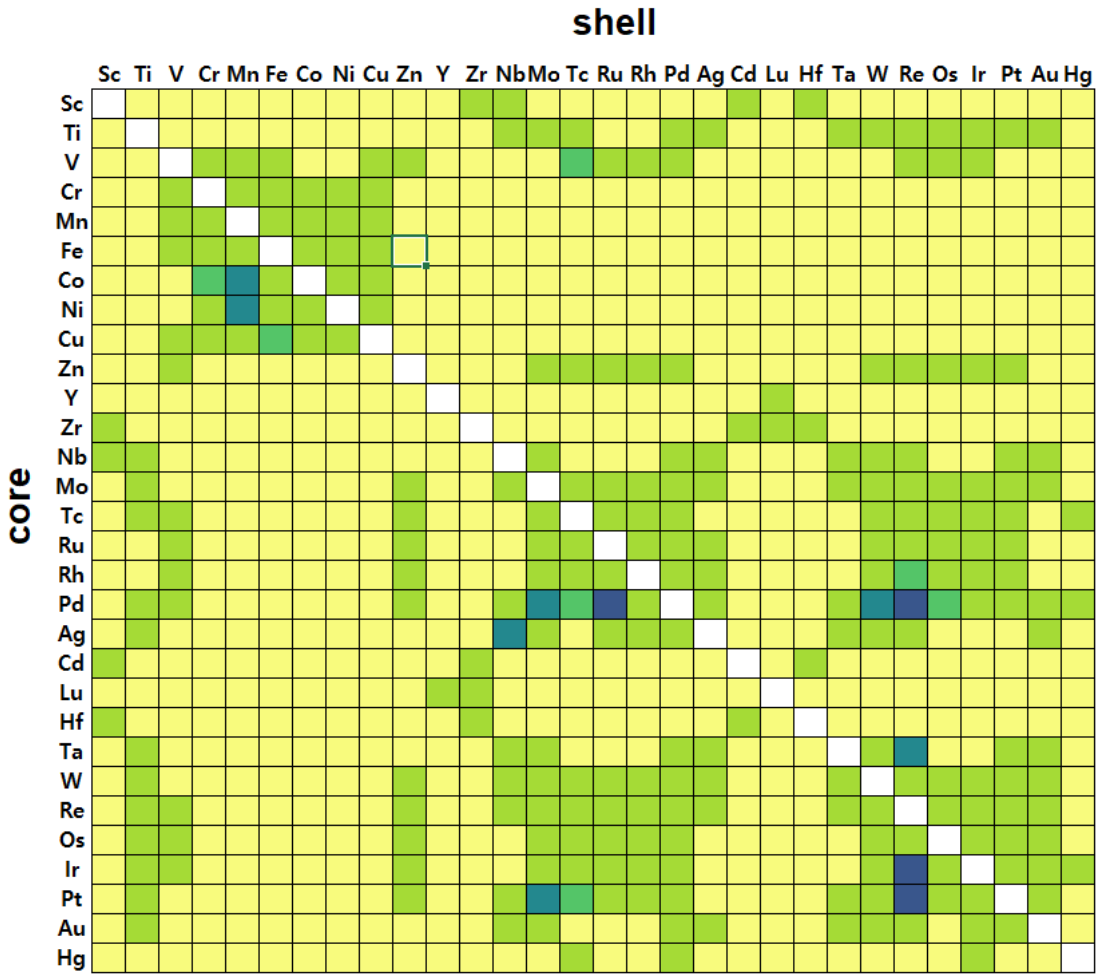

Fig. S3 Summary of the whole screening process to discover promising NRR bimetallic core-shell catalysts. Following the screening protocol shown in Fig. 1(a), each candidate is marked using the color code of the corresponding screening step. Yellow, yellowgreen, green, and teal colored ones represent candidates satisfying first, second, third, and fourth screening steps, respectively. Navy colored ones are the final four promising candidates, which are Pd-Ru, Pt-Re, Ir-Re, and Pd-Re.

Table S3. Free energy changes of reaction intermediates in Figs. 1 and 2. Units in eV.

Core-Shell	ΔG_{*N2}	ΔG_{*N2H}	ΔG_{*N2H2}	ΔG_{*N}	ΔG_{*NH}	ΔG_{*NH2}	ΔG_{*NH3}	ΔG_{*H}
Pd-Ru	-0.39	-0.10	-0.27	-1.29	-1.14	-0.90	-0.91	-0.50
Pt-Re	-0.27	0.02	-0.39	-1.05	-1.22	-0.93	-0.93	-0.56
Ir-Re	-0.17	0.31	-0.09	-0.87	-1.23	-0.87	-0.95	-0.45
Pd-Re	-0.26	0.06	-0.38	-1.05	-1.25	-0.92	-0.97	-0.51
Co-Mn	-0.13	-0.26	-0.13	-1.31	-1.58	-0.94	-0.84	-0.34
Pt-Mo	-0.31	-0.39	-0.36	-1.87	-1.45	-1.12	-0.20	-0.52
Pd-Mo	-0.29	0.27	0.21	-1.69	-1.76	-1.17	-0.15	-0.22
Ta-Re	-0.35	-0.69	-0.56	-1.47	-1.81	-1.26	0.19	-0.56
Ni-Mn	-1.32	-1.91	-1.08	-2.75	-3.04	-1.48	-1.89	-1.92
Pd-W	-0.30	-3.08	-3.16	-2.15	-2.02	-2.34	-2.85	-3.03
Ag-Nb	-0.16	-2.35	-2.12	0.93	1.06	-2.68	-0.81	-0.73
Pd-Ru(hcp)	-0.35	0.37	0.22	-1.18	-1.10	-0.83	-0.94	-0.42
Ru	-0.24	0.48	0.34	-1.07	-1.08	-0.74	-0.89	-0.39

Table S4. DFT results for the (a) Pd-Ru model under different strains (-5%, -3%, 0%, and +1%) and (b) Ru-shell catalysts with various core metals. The strain value (with respect to the unperturbed Pd-Ru), *d*-band center, ΔG_{*N2}, ΔG_{*H}, ΔG_S, and Bader charge change (Δq) are calculated for each catalyst. Δq is calculated with respect to Pd-Ru, $\Delta q = q_{(Pd\text{-}Ru)} - q_x$, where $q_{(Pd\text{-}Ru)}$ is the surface charge of Pd-Ru and q_x is the surface charge of catalyst x. Therefore, a more negative Δq suggests more surface charge loss than Pd-Ru, and vice versa.

(a)

	Strain (%)	*d*-band center (eV)	ΔG_{*N2} (eV)	ΔG_{*H} (eV)	ΔG_S (eV)
PdRu-5	-5	-1.244	-0.21	-0.42	0.21
PdRu-3	-3	-1.196	-0.26	-0.44	0.18
Pd-Ru	0	-1.120	-0.39	-0.50	0.12
PdRu+1	+1	-1.118	-0.53	-0.60	0.07

(b)

Core-shell	Strain (%)	*d*-band center (eV)	ΔG_{*N2} (eV)	ΔG_{*H} (eV)	Δq (e)
Ru	-3.12	-1.47	-0.24	-0.39	-0.08
Re-Ru	-2.16	-1.51	-0.28	-0.41	+0.11
Ir-Ru	-2.45	-1.36	-0.30	-0.42	-0.13
Al-Ru	+1.70	-1.16	-0.37	-0.45	+0.09
Pt-Ru	+0.18	-1.18	-0.41	-0.51	-0.005
Pd-Ru	0	-1.12	-0.39	-0.50	0

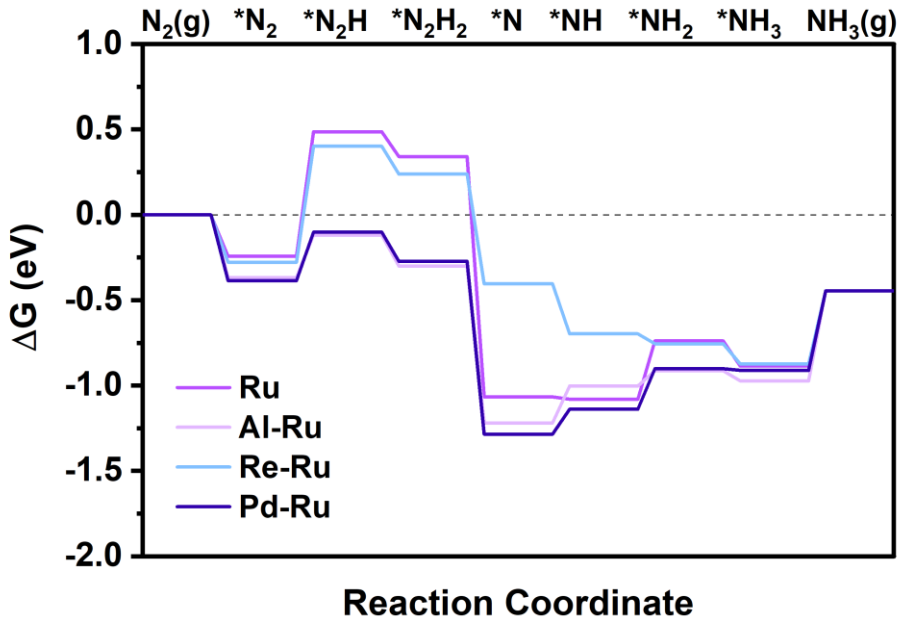

Fig. S4 Free energy diagrams for Ru-shell catalysts (Ru, Al-Ru, Re-Ru, and Pd-Ru) with different core metals.

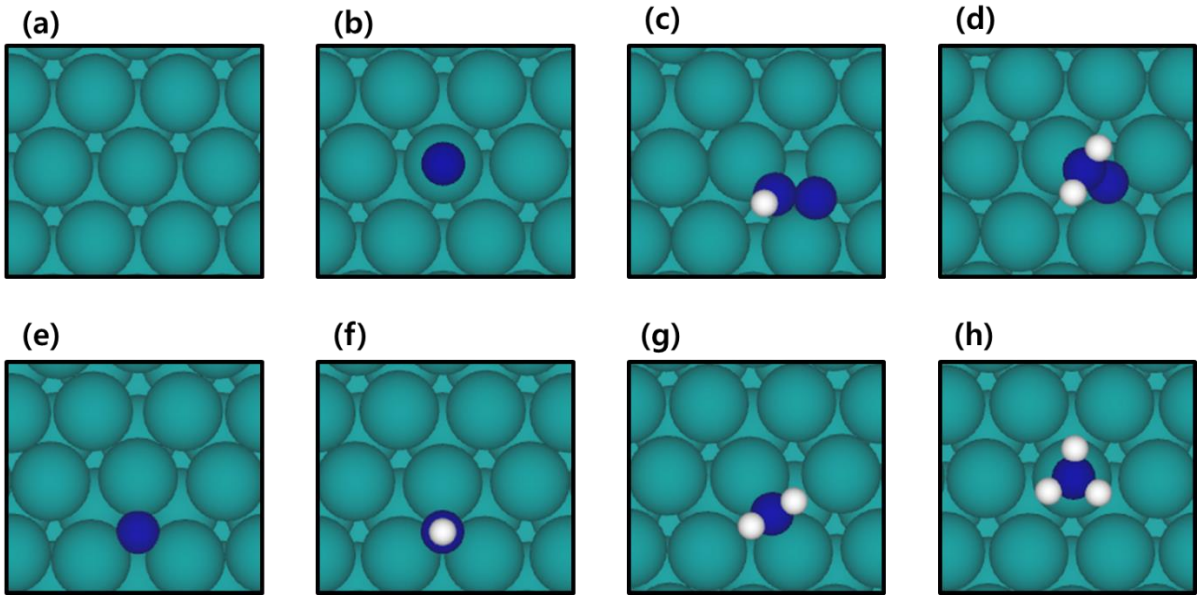

Fig. S5 Optimized adsorption geometries of the NRR intermediates on the Pd-Ru surface: (a) bare surface, (b) *N_2, (c) *N_2H, (d) *N_2H_2, (e) *N, (f) *NH, (g) *NH_2, and (h) *NH_3.

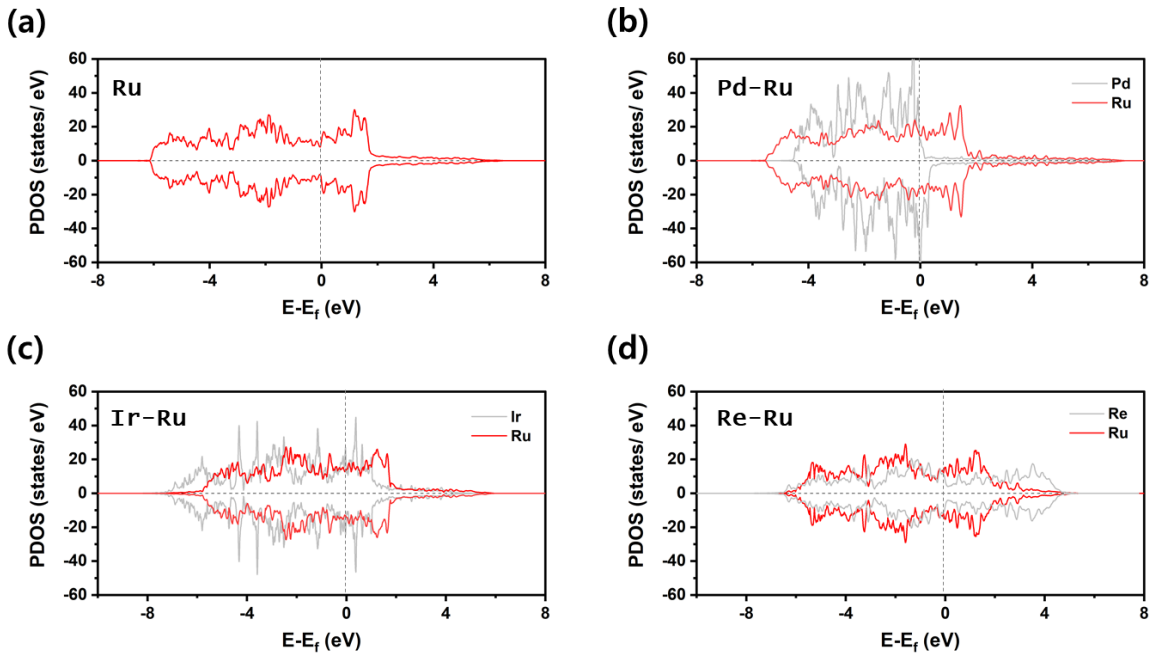

Fig. S6 PDOS of the Ru *d*-orbital for each catalyst: (a) Ru, (b) Pd-Ru, (c) Ir-Ru, and (d) Re-Ru. Ru *d*-orbitals are shown as red lines, and core-metal *d*-orbitals (Pd, Ir, or Re) are shown as gray lines. Positive and negative values of the y-axis represent the upper and lower spin states, respectively.

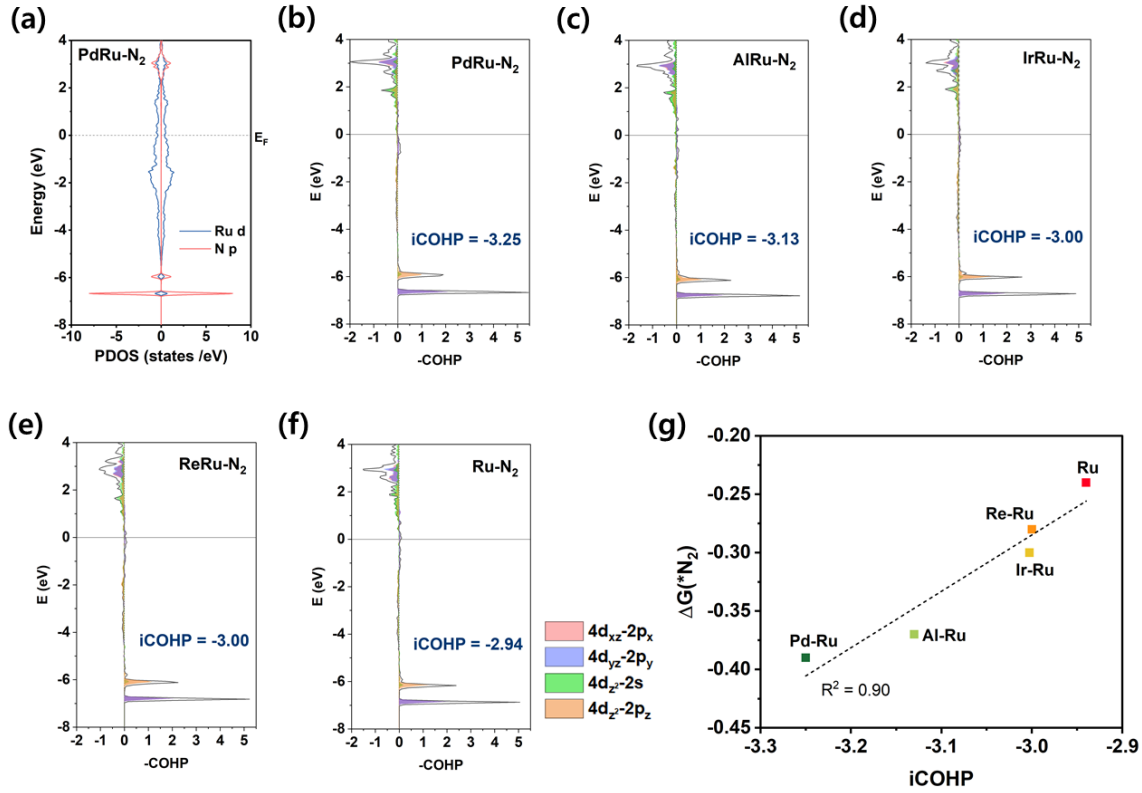

Fig. S7 (a) PDOS of N_2 on the Pd-Ru surface and (b–f) COHP plots of N_2-adsorbed M-Ru (M = Pd, Al, Ir, and Re) core–shell catalysts and pure Ru. (g) Linear correlation between ΔG_{*N2} and iCOHP for the tested Ru-shell catalysts.

Table S5. DFT results for (a) the Pd-Re model under different strains (-3%, -1%, 0%, and +1%) and (b) the Re shell catalysts with various core metals. The strain value (with respect to the unperturbed Pd-Re), *d*-band center, ΔG_{*N2}, ΔG_{*H}, ΔG_S, and Bader charge change (Δq) are calculated for each catalyst. Δq is calculated with respect to Pd-Re, $\Delta q = q_{(Pd\text{-}Re)} - q_x$, where $q_{(Pd\text{-}Re)}$ is the surface charge of Pd-Re, and q_x is the surface charge of catalyst x. Therefore, a more negative Δq indicates more surface charge loss than Pd-Re, and vice versa.

(a)

	Strain (%)	*d*-band center (eV)	ΔG_{*N_2} (eV)	ΔG_{*H} (eV)	ΔG_S (eV)
PdRe-3	-3	-0.62	-0.12	-0.44	0.32
PdRe-1	-1	-0.55	-0.22	-0.49	0.27
Pd-Re	0	-0.53	-0.26	-0.51	0.25
PdRe+1	+1	-0.51	-0.30	-0.53	0.23

(b)

Core-shell	Strain (%)	*d*-band center (eV)	ΔG_{*N_2} (eV)	ΔG_{*H} (eV)	Δq (e)
Pt-Re	0.2	-0.49	-0.27	-0.56	-0.05
Pd-Re	0	-0.53	-0.26	-0.51	0
Ir-Re	-2.4	-0.83	-0.17	-0.45	-0.09

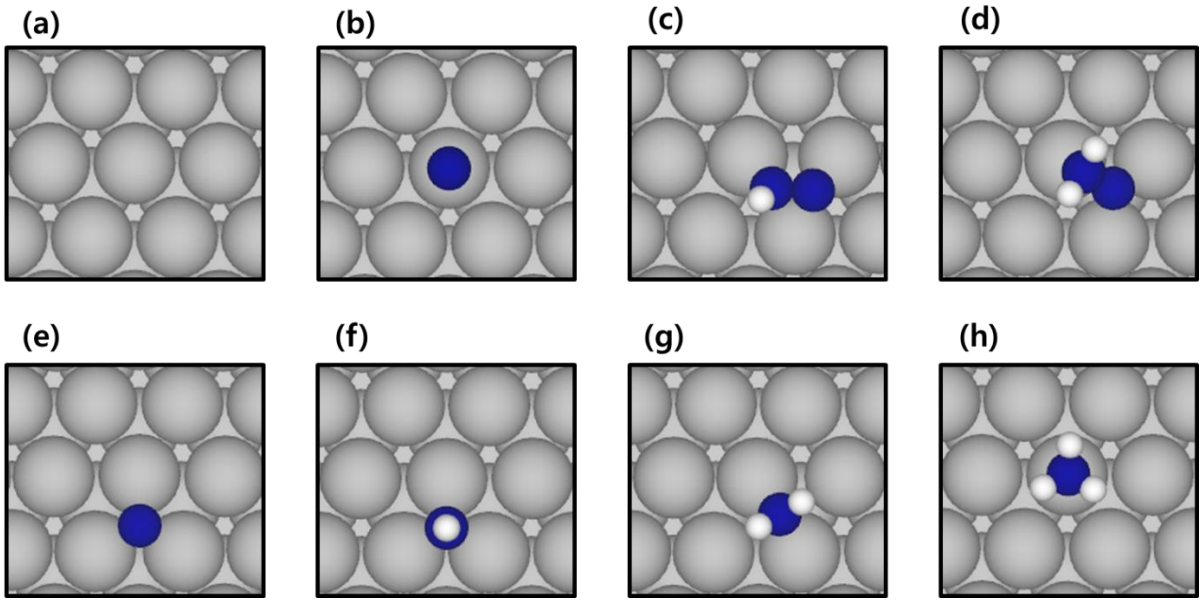

Fig. S8 Optimized adsorption geometries of the NRR intermediates on the Pd-Re surface: (a) bare surface, (b) $*N_2$, (c) $*N_2H$, (d) $*N_2H_2$, (e) *N, (f) *NH, (g) $*NH_2$, and (h) $*NH_3$.

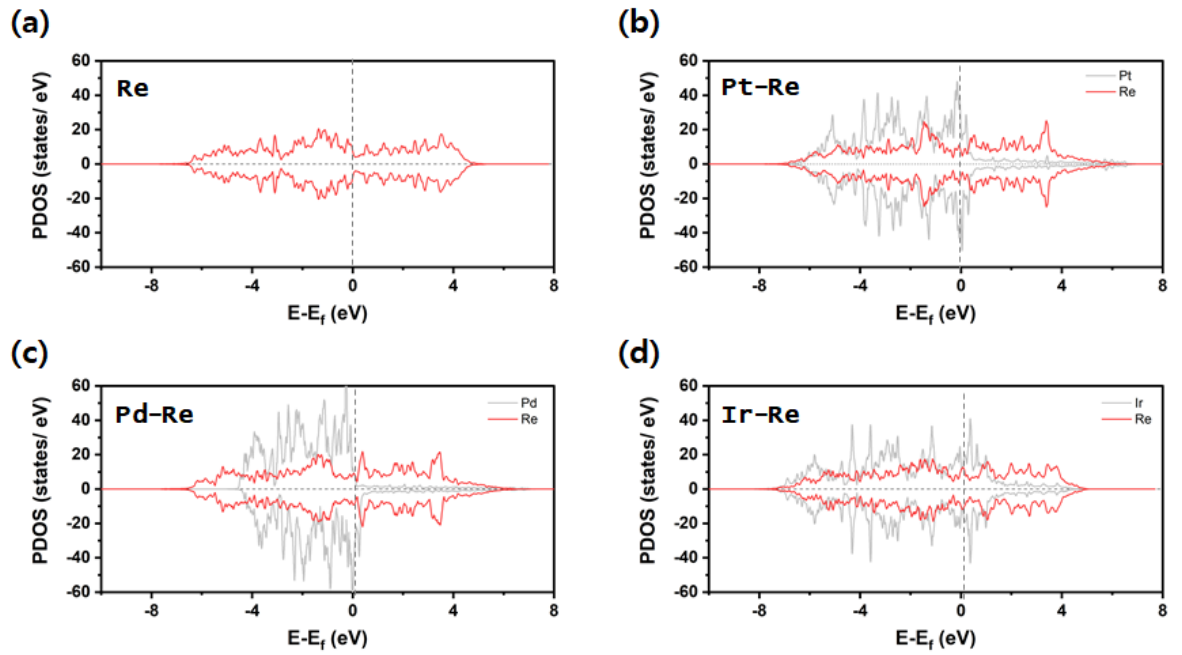

Fig. S9 PDOS of the Re *d*-orbital for each catalyst: (a) Re, (b) Pt-Re, (c) Pd-Re, and (d) Ir-Re. Re *d*-orbitals are shown as red lines, and core-metal *d*-orbitals (Pt, Pd, or Ir) are shown as gray lines. Positive and negative values of the y-axis represent the upper and lower spin states, respectively.

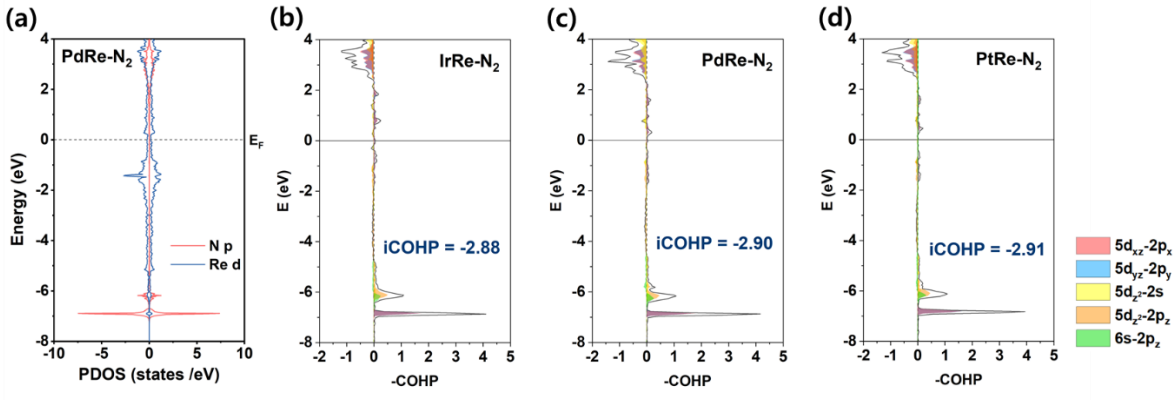

Fig. S10 (a) PDOS of *N_2 on the Pd-Re surface and (b–d) COHP plots of N_2-adsorbed M-Re (M = Ir, Pd, and Pt) core–shell catalysts.

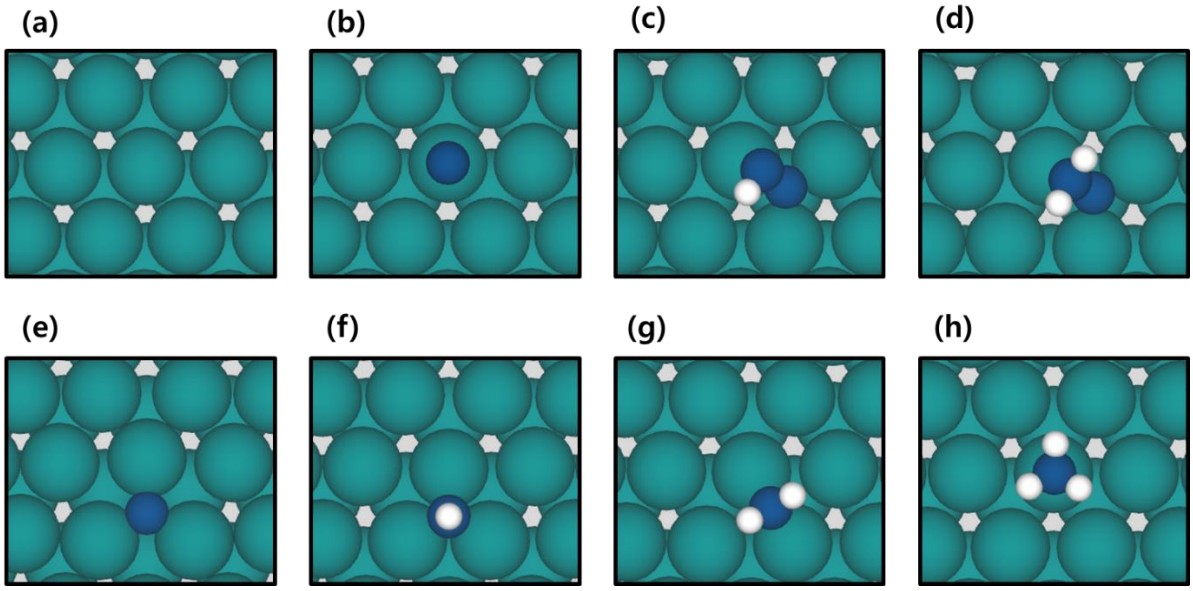

Fig. S11 Optimized adsorption geometries of the NRR intermediates on the Pd-Re-Ru surface: (a) bare surface, (b) $*N_2$, (c) $*N_2H$, (d) $*N_2H_2$, (e) *N, (f) *NH, (g) $*NH_2$, and (h) $*NH_3$.

Table S6. Free energy changes of reaction intermediates in Fig. 6. Units in eV.

Core-Shell	ΔG_{*N2}	ΔG_{*N2H}	ΔG_{*N2H2}	ΔG_{*N}	ΔG_{*NH}	ΔG_{*NH2}	ΔG_{*NH3}
Pd-Ru	-0.39	-0.10	-0.27	-1.29	-1.14	-0.90	-0.91
Pd-Re-Ru	-0.37	-0.07	-0.18	-1.03	-0.95	-0.82	-0.87

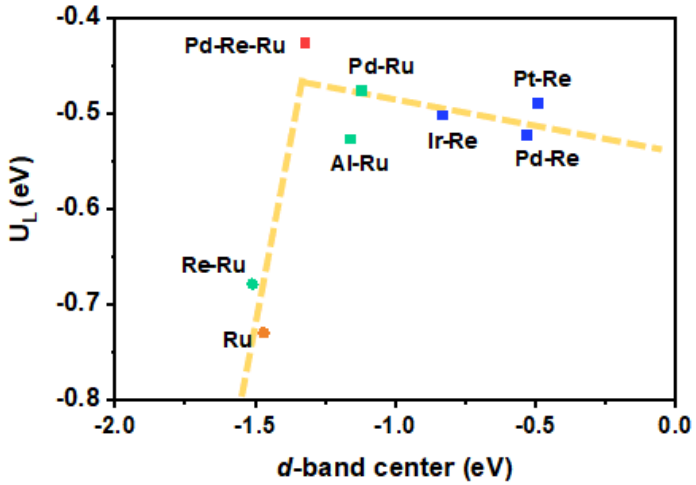

Fig. S12. U_L plotted against the d-band center for X-Ru and X-Re core-shell catalysts. Green for Ru-shell catalysts, blue for Re-shell catalysts, orange for pure Ru, and red for Pd-Re-Ru catalyst. The reactions with the first hydrogenation step ($*N_2$ → $*N_2H$) as the rate-determining step (RDS) are indicated by circles, while those with NH3 desorption step as the RDS are represented by squares.

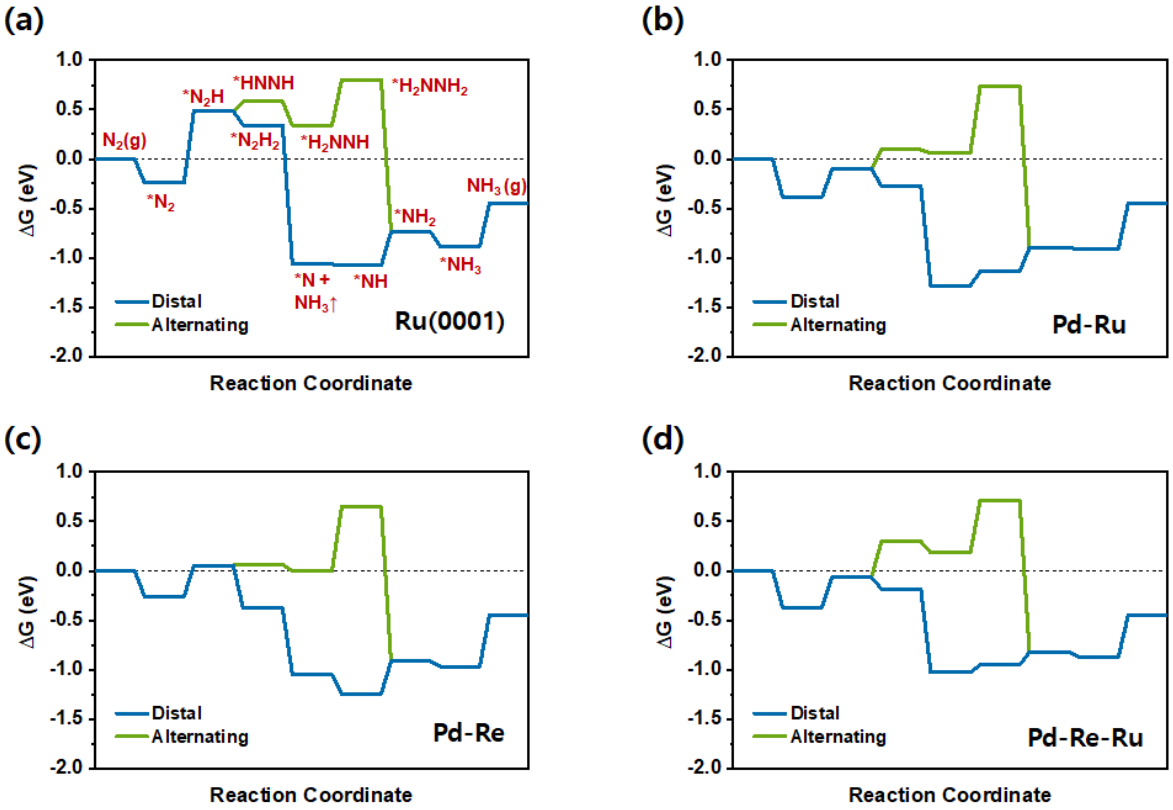

Fig. S13 NRR free energy diagrams along the distal and alternating pathways for a selection of catalysts: (a) Ru(0001), (b) Pd-Ru, (c) Pd-Re, and (d) Pd-Re-Ru.